# Development of a Versatile and Reversible Multi-Stack Solid Oxide Cell System Towards Operation Strategies Optimization



ECS Transactions, 111 (6) 1677-1688 (2023)
10.1149/11106.1677ecst ©The Electrochemical Society

# Development of a Versatile and Reversible Multi-Stack Solid Oxide Cell System Towards Operation Strategies Optimization

G. Cubizolles, S. Alamome, F. Bosio, B. Gonzalez, C. Tantolin, L. Champelovier, S. Fantin, and J. Aicart

Univ. Grenoble Alpes, CEA/LITEN, 17 rue des Martyrs, 38054 Grenoble Cedex 9, France

Solid oxide cell technology is currently experiencing a rapid industrialization phase. To investigate operational strategy, CEA/LITEN has designed and constructed its first multi-stack reversible solid oxide cell (rSOC) module. While it is able to host four of CEA's standard 25-cell stacks, the present work reports on preliminary validation results obtained in a 2-stack configuration. Thermal losses have been quantified and identified. While the hotbox is showing high performances, the overall losses increased twofold when taking into account pass-through piping and current connections. Module fluid distribution was verified to be homogeneous, and does not affect nominal stack operation. A durability test of more than 2 kh is presented. Over the first 1.1 kh, the stacks behavior was compared to that of a stack previously operated on a test bench. The remarkable similarities indicate adequate control of the module. Finally, a detailed analysis of the recorded efficiency was conducted.

## Introduction

High temperature electrolysis (HTE) based on solid oxide cell (SOC) technology is entering a global and dynamic industrialization phase, boosted by public investments and promises of game-changing efficiencies compared to the more market-ready technologies. Indeed, proton exchange membrane (PEM) and alkaline electrolyzes are expected to reach 70%$_{LHV}$ efficiencies by 2030, when HTE could reach 90%$_{LHV}$ if supplied with low-cost steam (1). Such significant efficiency boost compared to the low temperature technologies is particularly relevant in the current context of high electricity and natural gas prices. Consequently, Sunfire Gmbh, SolydEra (formerly SolidPower), Topsoe, Genvia, Ceres Power and Bloom Energy, among others, all have recently made big announcements regarding the development of their respective technologies (2–4). Overall, efforts are now devoted to turning these high theoretical efficiencies (low operational expenditure - OPEX) into low levelized cost of hydrogen (LCOH (5)) through minimizing capital expenditure (CAPEX). While modular approaches are typically adopted in (pre) industrial installations, these low cost, high efficiency objectives are tackled by increasing the power of modules through incorporation of a high number of cells and stacks. In this context, and to accompany the industrialization of HTE and its partners, CEA/LITEN has designed and built a highly instrumented, four-stack reversible module comprising a large number of functions and balance of plant (BoP) components: heat exchangers, process air blower, recirculation pumps, regulation valves, etc. By design, the reversible module can be

operated in electrolysis mode, as well as $H_2$, $CH_4$, or natural gas fuel cell modes. This preliminary work reports validation results, notably thermal identification of losses and fluidic stack distribution, as well as electrolysis operation and performance maps in a 2-stack configuration. Consequently, a simplified module architecture is detailed, focused on the electrolysis mode. Efforts are devoted to comparing stacks behavior in a module environment to in-house data obtained on test benches.

## Experimental

Module and stacks architecture

The following Figure 1 details the module's process flow diagram (PFD) simplified to its HTE configuration for visibility. Process air is supplied to the stacks from laboratory ambient by a blower (b, Celeroton), located downstream of a filtration step and a water-cooling stage (a, Air/cooling water @ 15°C HEX) to get rid of excess humidity. The blower being oversized, a by-pass loop was incorporated. Air heating is first done via recuperation from air exhaust through a high temperature heat exchanger (c, HEX, Kaori). An electrical heater (d, in-house designed, indirect heating with SiC heating element from Kanthal) then insures that the air stack inlet temperature is that of the stack. At the cathode compartment side, the $H_2O/H_2$ feed is brought up to stack temperature via two HEX in series (A & B, Bosal), to accommodate a pre-reformer in future work, as well as an electric heater (C, similar to d). Downstream from the stacks and both fuel HEXs, a cooling and separation stage – E – reduces the humidity down to <2 vol.% to prevent condensation in unwanted locations. At each of the module's gas outlets, two regulation valves with different *Kv* were installed to control the pressure levels and/or flowrates in the stack compartments and accommodate the large range of intended flowrates. The purpose-designed drop-down hot box can host four stacks disposed "two-over-two", and incorporates a few high temperature heating resistances – D. With its massive 350 mm insulation walls, it should allow investigating the interactions the stacks have on one another while controlled by thermal phenomena. This last point can typically not be studied on single-stack test benches, where thermal losses largely outweigh stack power, preventing them from heating up or cooling down electrochemically. The hot BoP components are individually insulated, and all are grouped in a casing filled with vermiculite granule materials located under the hotbox. To address safety issues, air within the furnace is constantly replenished to insure burning any $H_2$ leaks before ATEX formation (≈1.2 $Nm^3.h^{-1}$). Also, air around BoP components and in between the BoP and the hot box is pulled by an extractor (≈180 $m^3.h^{-1}$ at 20°C) instrumented with speed and gas sensors. These two airflows, impacting module efficiency, have yet to be optimized. In this preliminary work, only two stacks were integrated in the furnace, in top positions. These positions being numbered 1 and 3 in the module's frame of reference, the stacks will be denoted by S1 and S3 in the following. Dummy stacks, exhibiting the same size, mass, and overall heat capacity as the actual ones, filled the bottom slots.

The module is installed on CEA's Multistack platform, incorporating an in-house tweaked industrial steam generator supplied with deionized (DI) water, four 30 kW reversible power supplies (PSB-10200-420, Elektro Automatik), and different mass flow controllers connected to the multiple gas networks. Additional details on the platform and the DI water quality have been given in references (6) and (7), respectively. It should be

noted that due to the two-stack configuration and the flowrates being halved, the control over the steam supply performed below expectation, leading to ±5% fluctuations. Overall, the complete installation (module and hosting platform) incorporates 28 pressure and pressure drop sensors (2051 & 3051S, Emerson), 6 power-meters (Diris A-60, Socomec), 15 flowmeters and 5 composition analyzers of various technologies, 100+ type-K & type-N thermocouples (TC-Direct, Cat.1) and 100+ cell voltage measurements, among other sensors. A general view of the installation is given in Figure *2*.

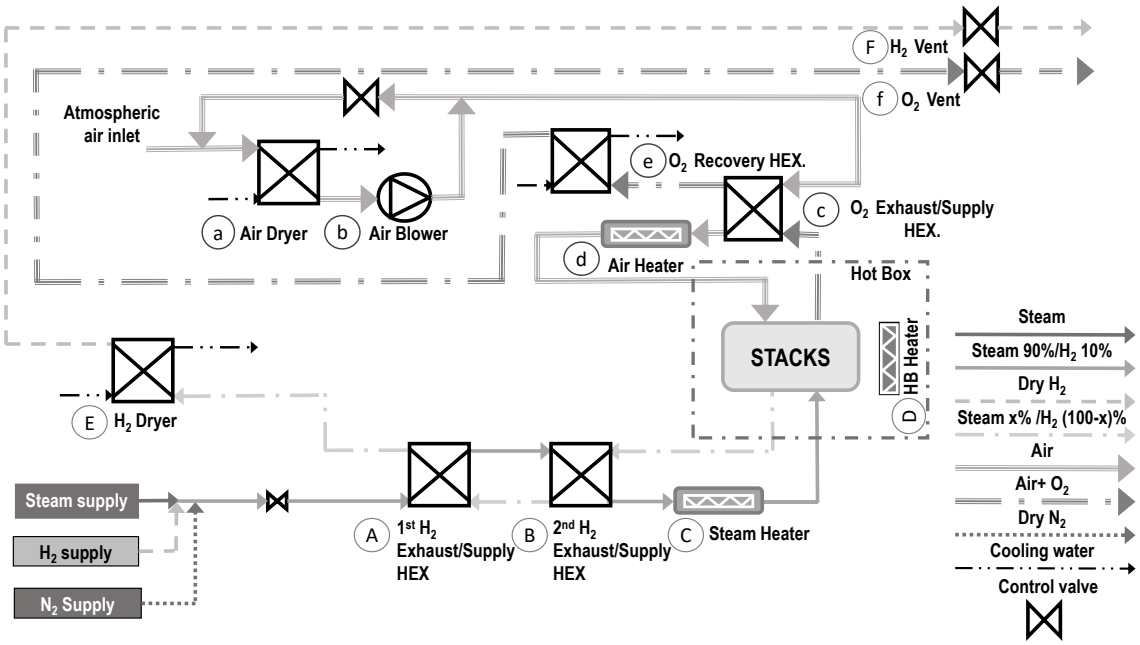


Figure 1. Process flow diagram of the four-stack reversible module, simplified to its electrolysis configuration.

Figure 2. Picture of the complete installation on the Multistack platform.

While ongoing efforts are devoted to upscale the base design (8), the module incorporates in its current configuration CEA's standard stacks. They comprise 25 commercial cathode-supported cells (Ni-YSZ/8YSZ/CGO/LSC) with a 100 cm² active surface, thin AISI441 ferritic stainless steel interconnects with proprietary design allowing for cross-flow operation, and an integrated stand-alone clamping system for mechanical load (9). Gas connection to the module is achieved using proprietary high temperature flanges (10). Additional information on stack design and experimental results on performance and durability can be found in references (5,11–15).

Stack operational strategy

Electrolysis operation was carried out by feeding the stacks with 90/10 vol.% $H_2O/H_2$ to prevent Ni oxidation in the hydrogen electrodes. A fast current transient strategy was adopted (approximatively ±1 $(A.cm^{-2}).min^{-1}$) when ramping up from open circuit (OCV) to near-thermoneutral voltages (6,7). At all times, the air compartment of the stacks was kept over-pressurized compared to the $H_2$ side via a combination of air inlet flowrate and back pressure valve adjustments. During stabilized operation under constant current, stack temperature was incrementally adjusted to compensate degradation and maintain thermoneutral voltage, insuring high DC-to-$H_2$ efficiency and preventing the establishment of thermal gradients within the stacks (7,15). While all stack currents are technically individually controlled, one of the base objective for this project is to investigate stacks arranged in series electrically (i.e. identical currents). Consequently, throughout this work, the two stack current set points have been kept identical, and the recorded difference between actual currents was negligible (<0.1%). Finally, performance maps were recorded following the method described in a previous work (6).

## Results and Discussion

Quantification of Thermal Losses

The thermal losses of the hotbox have been quantified at different steps of the assembly and for different operating temperatures, as shown in Figure 3. First, the losses were measured without any fluidic connection (C1-round markers) to qualify the insulation performance. This test highlighted a significant thermal inertia, with a time constant greater than 1 day. Consequently, it is important to underline that evaluating a steady state and precisely assess "actual" thermal losses is a difficult task, especially considering that boundary conditions have their own fluctuations throughout the day. Nevertheless, the orders of magnitude could be established. Then, all pass-through piping was installed, and the measurements redone (C2-black squared markers). Inertia was made evident in Figure 3 by superimposing the recorded data for thermal losses over the ten preceding hours leading to the measurement (empty squares), highlighting significant variations before stabilizing. It should be noted that the design of the module includes a high temperature air exchanger inside the HB, to later on investigate heat extraction strategies in SOFC mode. While not used here, its piping connections did impact heat losses. In this configuration, the corresponding heat losses (typically 920 W @ 700°C) were increased by more than 30% compared to the hotbox initial qualification. The third set of data takes into account the current connections and both the hotbox and the BoP safety air sweeps (C3-grey squared markers). Since each stack currents can be independently controlled, eight

connections are passing through the insulation. Having an air flow between the BoP and the hotbox did increase the overall heat losses, but the effect of the hotbox air sweep remained preponderant. For example at 700°C, the power to heat the air sweep was 310 W. One might expect to have larger heat losses in this third configuration, at least 920+310=1,230 W. In practice, these losses were closer to 1,150 W. This behavior, better than expected, is probably due to the exhaust of the hot air sweep, mainly located close to the piping and current connections passing through the insulation, consequently minimizing their respective impact. The last set of data in Figure 3 relates to the total power consumption of high temperature heaters in electrolysis operation (C4-triangular empty markers). Since the stacks were operated near the thermo-neutral voltage, they can be considered adiabatic. Consequently, the global thermal behavior of the hotbox is close to that obtained in the third configuration, confirming the order of magnitude of the overall heat losses then recorded. By differentiation, the contribution of (i) the thermal enclosure, (ii) the pass-through piping, and (iii) the current connection and safety sweeps can be identified and used to discuss the thermal performance of the system.

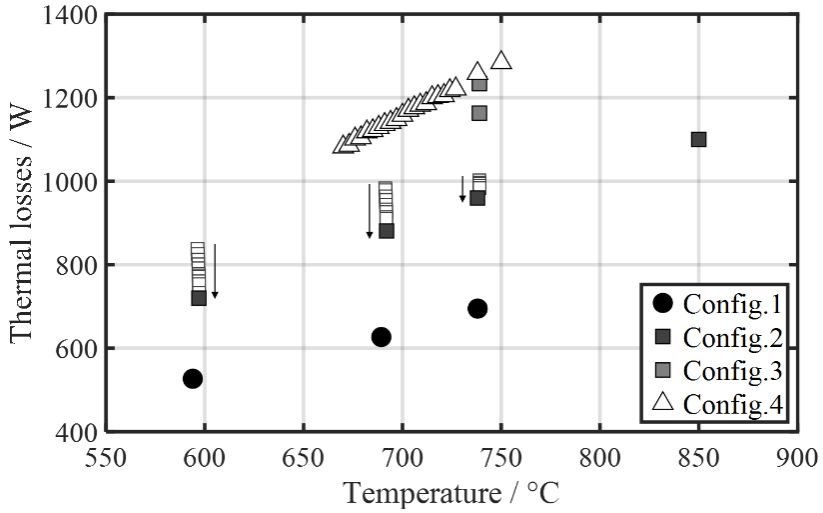


Figure 3. Thermal losses of the Hotbox in different configurations – $C_i$: 1) Thermal enclosure alone, 2) $C_1$ + pass-through piping, 3) $C_2$ + current connections and safety air sweeps, 4) $C_3$ + 2 stacks operated in thermoneutral conditions. For 3 data points of $C_2$, data over the 10 preceding hours is also given.

## Characterization of Stack Tightness and Fluidic Distribution

Initial maximum/average/minimum open circuit voltages (OCV) at approximatively 700°C and 1 NmL.min$^{-1}$.cm$^{-2}$ of dry $H_2$ were 1.08/1.14/1.18 V for S1 and 1.12/1.15/1.18 V for S3. Under such a low flowrate of $H_2$, this result denotes adequate overall tightness for both stacks, although a slight defect was detected on one cell of S1.

Figure 4 displays SOFC-$H_2$ and SOEC polarization curves obtained simultaneously on both stacks at 700°C. For the former, a maximum fuel utilization (FU) well above 90% was recorded at an average cell voltage of ≈0.84 V, consistent with previous works (12,14). In this specific case, a current ramp rate of +0.10 A.cm$^{-2}$.min$^{-1}$ was then used. A slight dissymmetry in the fuel distribution within the stacks is noticed, with the cell voltage dispersion increasing above 80% FU. Nevertheless, S1 and S3 displayed almost identical

behavior over the complete recording. In electrolysis mode, stack behaviors were also remarkably similar, and a steam conversion (SC) greater than 80% was recorded at the thermoneutral voltage. Overall, the results of this paragraph suggest (i) that the flowrate feeding the Ni-YSZ electrodes is well distributed to the stacks within the module, (ii) adequate flow distribution within the stack, (iii) and excellent initial cell performance at 700°C. It is important to underline that such conclusions can only be reached with robust processes for cells and stacks manufacturing.

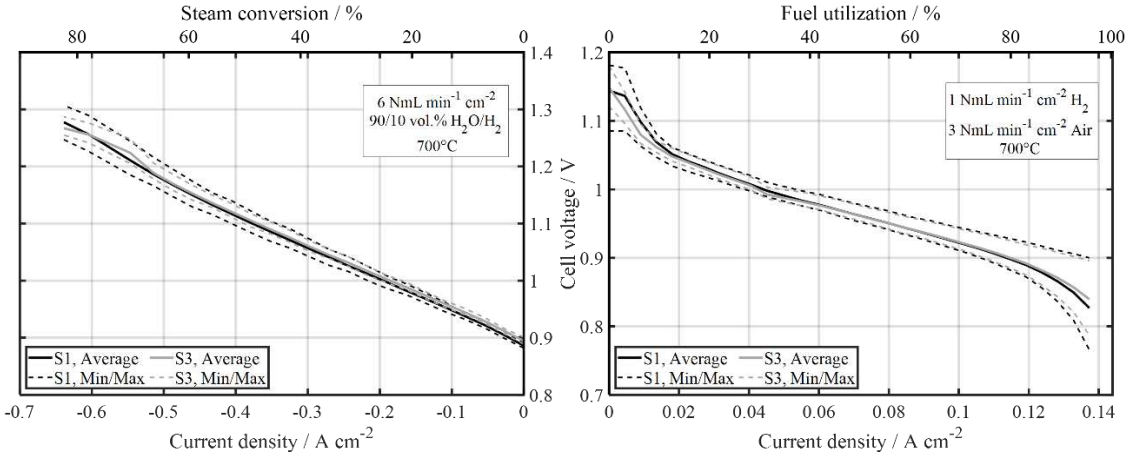


Figure 4 : Polarization curves in SOEC mode (left) and SOFC-$H_2$ mode (right).

Stack Operation at -0.65 A.cm$^{-2}$ and ≈70% Steam Conversion

After the initial characterizations, the two stacks were operated for approximately 1,300 h under constant current density (-0.65 A.cm$^{-2}$) and steam conversion (SC ≈70%), while incrementally increasing stack temperature to maintain thermoneutral voltage. The objective here was to compare their overall behavior within the module environment to that of an "as-identical-as-can-be" stack previously operated on a test-bench in similar conditions (15). Results, displayed in Figure 5, show a rapidly evolving stack temperature over the first ≈1 kh of testing, consistent with several literature reports (14,16). S1 and S3 temperature evolutions were strictly similar and equals at ±5°C. This behavior is also strikingly similar to the data of (15), also reported in Figure 5 for simplicity, emphasizing here again highly reproducible stack behavior and underlying manufacturing processes. An important distinction between the operating conditions in (15) and this work relates to the air supply: the test bench was fed with dry air (1.1.1 according to ISO8573-1 :2010) while the module supplies the stacks with (winter) ambient air cooled to 15°C only. While cold months rarely carry high levels of humidity, this preliminary result suggests a tolerance of the cells (mainly) to low levels of humidity in SOEC mode, or at the very least, that the impact is not significant compared to other phenomena affecting the stacks' response over the first ≈1,000 h of operation.

Following these measurements, different parametric investigations around control loops were carried out, while modifications of the steam feed were implemented to increase stability. For example, from 1,300 to 1,500 h, the overall HB temperature was increased so that the average cell voltage dropped from 1.29 to 1.27 V. Overall, at the time of writing this paper, the stacks have been in operation for approximatively 2 kh.

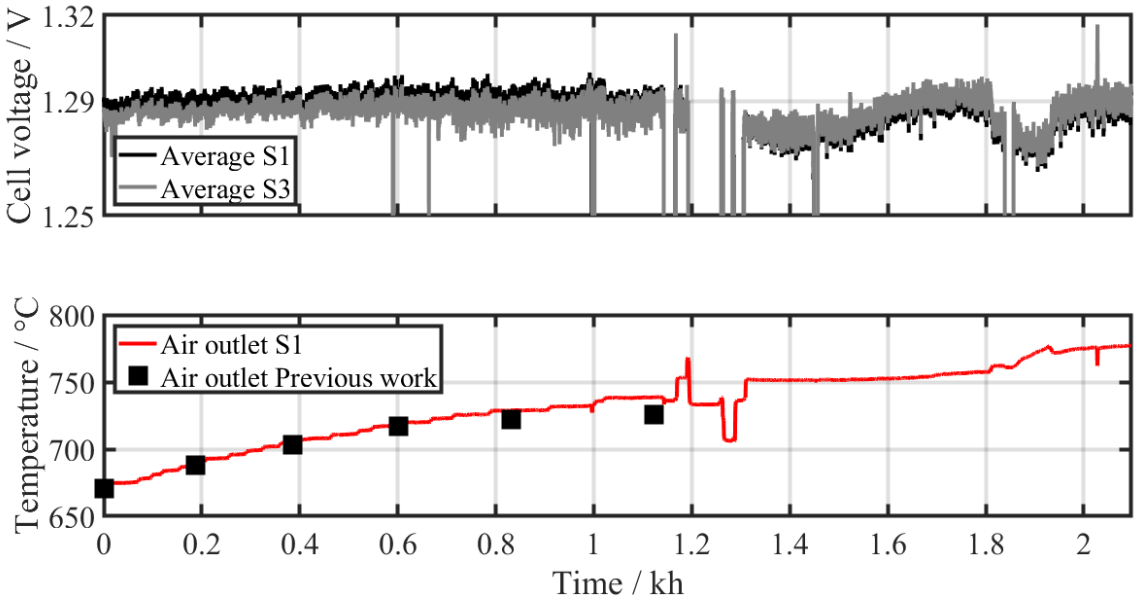


Figure 5. Time evolutions of S1 and S3 average cell voltage (up), and S1 temperature defined as the outlet air temperature. Data from (15) is also shown.

Performance map

From about 1,100 to 1,300 h, a performance map was recorded. For different conditions of targeted stack temperatures, the $H_2/O_2$ flowrate and the current density were incrementally adjusted to simultaneously observe (i) targeted temperature, (ii) targeted SC, and (iii) near-thermoneutral voltage. Given that the stacks behavior in the module environment was very close to that recorded on the test bench, the main objective was here to record the performances after the initial rapid evolution of stack temperature had stabilized, and compare the results to that of (15). Results corresponding to 70% SC between -0.5 and -1 $A.cm^{-2}$ are presented in Figure 6, along with data from (15) recorded in similar conditions, both initially and after 6,800 h of operation.

Results show a significant decrease of performance between data recorded initially and at 1,100 h, as illustrated by the substantial temperature increase at iso-current. Conversely, the difference in performance between 1,100 h and 6,800 h is much less pronounced, suggesting that most of the stack degradation comes from the first ≈1 kh of operation, and that beyond, the stacks degrade at a much slower rate. However, these preliminary observations need additional work for further validation.

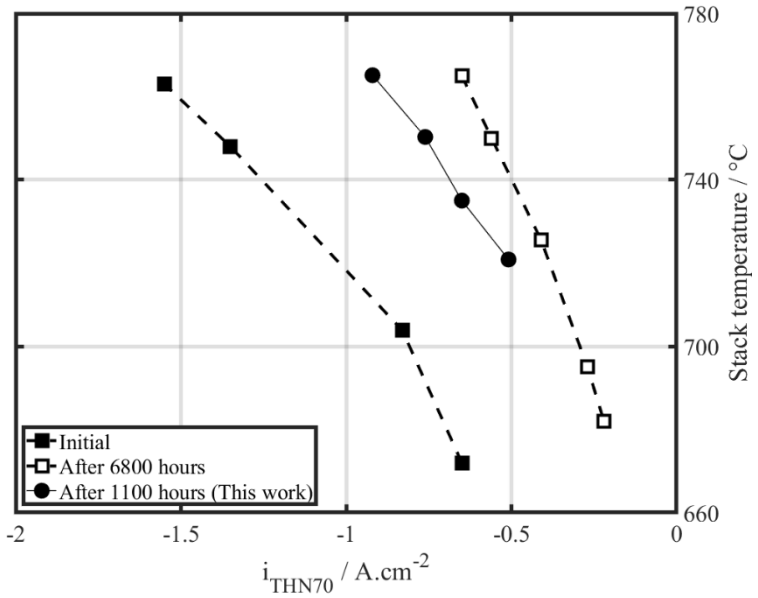


Figure 6. Performance map at ≈ 70% SC recorded after 1.1kh of operation at -0.65 A.cm$^{-2}$ (round markers). Results of (15) recorded initially and after 6,800 h are also reported (square markers).

Detailed efficiency measurements

Figure 7 details the system efficiency in a 2-stack configuration, in specific operating conditions (-0.65 A.cm$^{-2}$, SC≈70%), and after about 1,100 h of electrolysis operation (735°C). The overall efficiency based on the lower heating value (LHV) was 44% when including steam production, and 51% without. The power distribution showed a large contribution of the heaters (air, steam and hotbox heaters) whereas the contribution of the mechanical parts (air and ATEX blower) remained quite small. The power consumption of heating wires, required for thermal regulation of the fuel piping to prevent water condensation, have been included. Indeed, condensation is to be avoided, as instant re-vaporization can lead to pressure events, damaging the sealing of the stacks and/or their electrical contacts. The piping connected to pressure sensors are also temperature-controlled, and included in this thermal balance. In total, its impact on overall power consumption was significant (9% of the system), even if some of the piping were not use in this configuration (no recirculation loop for example). The hotbox heaters power corresponds to the heat losses of the hotbox but also include both the heating of the air sweep (about 330 W) and the final preheating of the process gases.

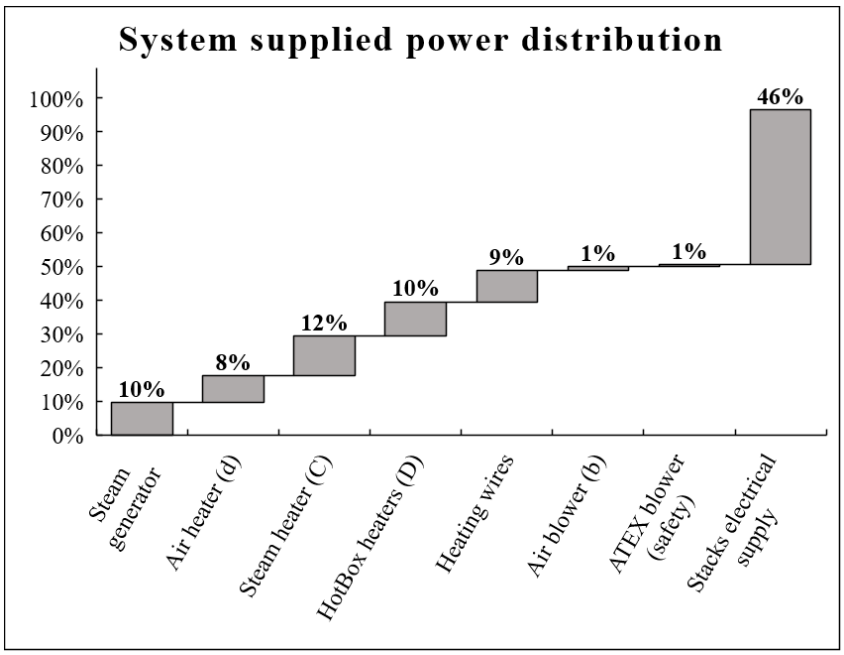


| Operating point | | |
|---|---|---|
| i = | 0,65 | A/cm² |
| SC ≈ | 70 | % |
| T = | 735 | °C |

| Power balance | | |
|---|---|---|
| **Supplied power** | | |
| Steam generator | 873 | W |
| Air heater (d) | 725 | W |
| Steam heater (C) | 1071 | W |
| HotBox heaters (D) | 1268 | W |
| Heating wires | 836 | W |
| Air Blower (b) | 115 | W |
| ATEX Blower (safety) | 50 | W |
| Stacks electrical supply | 4188 | W |
| **Total** | **9126** | **W** |
| **Collected power** | | |
| **$H_2$ produced (LHV)** | **4078** | **W** |
| **System efficiency** | | |
| Steam production | **η LHV** | |
| Included | **44%** | |
| Not included | **51%** | |

Figure 7. Efficiency breakdown in a 2-stacks configuration. Component nomenclature refer to Figure 1.

The low global efficiency that these first results yielded can be explained by the test bench conception, targeting multiple operating modes and fuels, as well as a large range of flowrates. The following discussion highlights three major contributions.

First, as mentioned before for the preheating of the steam/hydrogen mixture, two HEX have been installed in series (A & B, Figure 1) to accommodate a pre-reformer in future tests. A detailed analysis of their performances shows that they are quite oversized in regards to the 2-stack configuration and investigated operating conditions. Indeed more than 90% of the heat exchange for the steam preheating was performed only by one HEX. The second one did allow some furthering of the steam preheating, but more importantly induced greater heat losses. For both HEX, heat losses were about 44% of the power required for the steam preheating. A design dedicated to this specific operating point would have led to have just one smaller HEX. When four stacks will be incorporated in the module, heat losses of both HEX are expected to drop to about 26% of the power necessary to preheat the steam inlet.

A second point to consider is the performance of both steam and air heaters (d and C, Figure 1). An analysis of their efficiency, meaning the ratio between the power required to heat the flowrates over their electrical power consumption, yielded 22% for the air heater and 32% for the steam heater. Unsurprisingly, the indirect heating design of the heaters, chosen to avoid contaminating the inlet gases, lowered their efficiency. As expected, the recorded efficiency was higher for the steam heater. The heat demand is higher on the steam side due to the mass flow unbalance between the inlet ant outlet, all-the-while losses are somewhat constant. Indeed, heat losses of both heaters were almost the same, and totaled up to 1,200 W. This significant contribution represented about 13% of the system overall power.

Finally, the air sweep flowing between the hotbox and the BoP is likely cooling the inlet gases before entering the hotbox. The corresponding heat losses are difficult to estimate,

and the gases are reheated via the piping inside the hotbox. Eventually, the heat losses in the piping outside the hotbox are compensated by the heaters located inside.

The above discussion highlights some abnormal heat losses, specific to the test bench. These, however, can easily be avoided in larger and (pre) industrial systems. Switching the module to a 4-stack configuration will not reduce the heat losses, which will remains almost constant, but such configuration will reduce their overall weight in the global system efficiency. At the very least, these preliminary results highlight the importance further gathering and integrating the high temperature components (stacks, preheating heat exchanger, and gas heaters) if maximizing the overall efficiency is the main objective.

As stated, future operation with 4 stacks will allow improving the global efficiency of the system. It is currently expected to be around 55%$_{LHV}$ when steam production will be included and 65%$_{LHV}$ without. In any cases, the efficiency may still remain far from that of a fully integrated module. Indeed, Peters et al. (17) reported an impressive 70%$_{LHV}$ for their 4-stack system. Nevertheless, optimisation paths have been clearly identified and will be implemented on future installations that target high efficiency.

## Conclusions

To support some of the challenges of an industrializing SOC technology, CEA/LITEN has designed and built its first multi-stack reversible module. Currently operable in SOEC, SOFC-$H_2$, SOFC-$CH_4$ and SOFC-natural gas modes, it was designed to incorporate four of CEA's standard cathode-supported stacks for a combined ≈10 $kW_{DC}$ nominal electrolysis power.

Thermal losses were initially quantified and identified, although the inertia and significant time constant impacted the measurements accuracy. While the thermal enclosure itself was found to be quite performant, the overall losses of the hotbox increased twofold when taking into account the pass-through piping, the numerous current connections, and the safety air sweeps. Unsurprisingly, the stack operating temperature also affected the overall thermal efficiency. Two stacks were then installed, and the remaining two slots filled with dummy stacks. The stacks showed excellent performances and adequate initial tightness and internal fuel distribution. Polarization curves recorded simultaneously and up to high fuel utilization or steam conversion showed good distribution of reactants over both stacks, a necessary condition for nominal operation. A 2 kh galvanostatic step at -0.65 $A.cm^{-2}$ and approximatively 70% SC was then started. Over time, stack temperature was gradually increased to compensate degradation. Data recorded over the first 1 kh was remarkably similar to that of a stack operated in a previous work on a test bench in similar condition. This showed that the impact of low levels of humidity in the inlet air was not significant compared to the other phenomena affecting the stacks' response over the first 1,000 h of operation, and could suggest a tolerance to low levels of humidity in the air supplied to the $O_2$ electrode. Preliminary comparison of performance data and its evolution over time would suggest that the stacks suffer significant degradation over the first 1 kh of operation, yet degrade at a much slower rate beyond that. Finally, a detailed analysis of the efficiency of the overall system was carried out. At 735°C, 75% SC and -0.65 $A.cm^{-2}$, efficiencies of 44 and 51 %$_{LHV}$ were recorded when taking or not taking into account the generation of steam, respectively. This result is a consequence of (i) the large number of functionalities the module integrates, (ii) suboptimal thermal integration of high temperature components, (iii) design choices for gas preheaters, and

(iv) overall balance of plant components not designed for the low flowrates of the 2-stack configuration.

The immediate next steps will remain centered on the electrolysis mode, and include the investigation of recirculation loops, allowing for self-sufficient operation in regards to the $H_2$ supply. Automatic and safe power level transitions are also targeted, before moving on to a four-stack configuration. Once optimized and fully operational, the installation should prove to be a valuable investigation tool for validating operation strategies and control loops, while generating detailed data for system modeling validation.

## Acknowledgments

The authors gratefully acknowledge that this work was financially supported by CEA and GENVIA. The Module development has also been partially supported by the REVERSI ADEME project. Data for the 25-100 reference stack presented in figures 5 and 6 have been obtained thanks to the funding from the Fuel Cells and Hydrogen 2 Joint Undertaking (now Clean Hydrogen Partnership) to the MULTIPLHY project under Grant Agreement No 875123.

## References

1. *Strategic Research and Innovation Agenda*, Hydrogen Europe, (2020).
2. K. Schwarze, T. Geißler, and R. Blumentritt, in *15th European SOFC & SOE Forum*,, vol. A1503, p. 543–552, Lucerne, Switzerland (2022).
3. https://https://multiplhy-project.eu/.
4. P. Tochon, C. Festa, N. Agrane, G. Iafrate, V. Mondelli, J. Aicart and D. Snoswell, in *15th European SOFC & SOE Forum*,, vol. A0602, p. 1–10, Lucerne, Switzerland (2022).
5. M. Reytier, S. Di Iorio, A. Chatroux, M. Petitjean, J. Cren, M. De Saint Jean, J. Aicart and J. Mougin, *Int. J. Hydrog. Energy*, **40**, 11370–11377 (2015).
6. J. Aicart, Z. Wuillemin, B. Gervasoni, D. Reynaud, F. Waeber, C. Beetschen, Y. Antonetti, A. Nesci and J. Mougin, *Int. J. Hydrog. Energy*, **47**, 3568–3579 (2022).
7. J. Aicart, L. Tallobre, A. Surrey, D. Reynaud, and J. Mougin, in *15th European SOFC & SOE Forum*,, vol. A0808, p. 151–162, Lucerne, Switzerland (2022).
8. S. Di Iorio, T. Monnet, G. Palcoux, L. Ceruti, and J. Mougin, in *15th European SOFC & SOE Forum*,, vol. A0904, p. 1–13, Lucerne, Switzerland (2022).
9. M. Reytier, C. Bernard, and P. Giroud, WO2017102657A1 (2017).
10. M. Planque, B. Oresic, G. Roux, P. Szynal, and C. Bernard, WO 2018/122531 (2017).
11. J. Mougin, S. Di Iorio, A. Chatroux, T. Donnier-Marechal, G. Palcoux, M. Petitjean and G. Roux, *ECS Trans.*, **78**, 3065–3075 (2017).
12. J. Aicart, S. Di Iorio, M. Petitjean, P. Giroud, G. Palcoux and J. Mougin, *Fuel Cells*, **19**, 381–388 (2019).
13. G. Cubizolles, J. Mougin, S. Di Iorio, P. Hanoux, and S. Pylypko, *ECS Trans.*, **103**, 351–361 (2021).
14. A. Hauch, A. Ploner, S. Pylypko, G. Cubizolles, and J. Mougin, *Fuel Cells*, **21**, 467–476 (2021).

15. J. Aicart, A. Surrey, L. Champelovier, K. Henault, C. Geipel, O. Posdziech and J. Mougin, in *15th European SOFC & SOE Forum*,, vol. A0804, p. 138–149, Lucerne, Switzerland (2022).
16. Y. Yang, X. Tong, A. Hauch, X. Sun, Z. Yang, S. Peng and M. Chen, *Chem. Eng. J.*, **417**, 129260 (2021).
17. Ro. Peters, M. Frank, W. Tiedemann, I. Hoven, R. Deja, N. Kruse, Q. Fang, L. Blum and R. Peters, *J. Electrochem. Soc.*, **168**, 014508 (2021).